



## Article

# New Cyanido-Bridged Heterometallic 3d-4f 1D Coordination Polymers: Synthesis, Crystal Structures and Magnetic Properties

Diana Dragancea<sup>1,2,\*</sup>, Ghenadie Novitchi<sup>3,\*</sup> , Augustin M. Mădălan<sup>1</sup> and Marius Andruh<sup>1,\*</sup>

<sup>1</sup> Inorganic Chemistry Laboratory, Faculty of Chemistry, University of Bucharest, Str. Dumbrova Rosie nr. 23, 020464 Bucharest, Romania; augustin.madalan@chimie.unibuc.ro  
<sup>2</sup> Institute of Chemistry, Str. Academiei nr. 3, MD 2028 Chişinău, Moldova  
<sup>3</sup> CNRS, University Grenoble Alpes, LNCMI, F-38000 Grenoble, France  
\* Correspondence: ddragancea@gmail.com (D.D.); ghenadie.novitchi@lncmi.cnrs.fr (G.N.); marius.andruh@dnt.ro (M.A.)

**Abstract:** Three new 1D cyanido-bridged 3d-4f coordination polymers,  $\{[\text{Gd}(\text{L})(\text{H}_2\text{O})_2\text{Fe}(\text{CN})_6]\cdot\text{H}_2\text{O}\}_n$  ( $1_{\text{GdFe}}$ ),  $\{[\text{Dy}(\text{L})(\text{H}_2\text{O})_2\text{Fe}(\text{CN})_6]\cdot 3\text{H}_2\text{O}\}_n$  ( $2_{\text{DyFe}}$ ), and  $\{[\text{Dy}(\text{L})(\text{H}_2\text{O})_2\text{Co}(\text{CN})_6]\cdot\text{H}_2\text{O}\}_n$  ( $3_{\text{DyCo}}$ ), were assembled following the building-block approach (L = pentadentate *bis*-semicarbazone ligand resulting from the condensation reaction between 2,6-diacetyl-pyridine and semicarbazide). The crystal structures consist of crenel-like  $\text{Ln}^{\text{III}}\text{-M}^{\text{III}}$  alternate chains, with the  $\text{Ln}^{\text{III}}$  ions connected by the hexacyanido metalloligands through two *cis* cyanido groups. The magnetic properties of the three complexes have been investigated. Field-induced slow relaxation of the magnetization was observed for compounds  $2_{\text{DyFe}}$  and  $3_{\text{DyCo}}$ . Compound  $3_{\text{DyCo}}$  is a new example of chain of Single Ion Magnets.

**Keywords:** heterometallic complexes; cyanido-bridged complexes; coordination polymers; single molecule magnets; lanthanides



**Citation:** Dragancea, D.; Novitchi, G.; Mădălan, A.M.; Andruh, M. New Cyanido-Bridged Heterometallic 3d-4f 1D Coordination Polymers: Synthesis, Crystal Structures and Magnetic Properties. *Magnetochemistry* **2021**, *7*, 57. <https://doi.org/10.3390/magnetochemistry7050057>

Academic Editors: Lee Martin, Scott Turner, John Wallis, Hiroki Akutsu and Carlos J. Gómez García

Received: 8 April 2021  
Accepted: 26 April 2021  
Published: 28 April 2021

**Publisher's Note:** MDPI stays neutral with regard to jurisdictional claims in published maps and institutional affiliations.



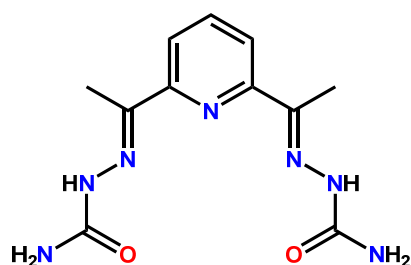
**Copyright:** © 2021 by the authors. Licensee MDPI, Basel, Switzerland. This article is an open access article distributed under the terms and conditions of the Creative Commons Attribution (CC BY) license (<https://creativecommons.org/licenses/by/4.0/>).

## 1. Introduction

The discovery of slow relaxation of the magnetization phenomena for discrete metal complexes (Single Molecule Magnets, SMMs) and 1D coordination polymers (Single Chain Magnets, SCMs) has stimulated the development of an intensive interdisciplinary research field. Beyond their relevance in fundamental Physics and Chemistry, spectacular applications in quantum computing and high-density information storage from these molecules are expected [1]. Although the field of SMMs was initially dominated by transition metal-based-systems, the focus of research shifted to lanthanides, which increase the energy barriers of SMMs [2,3]. The lanthanide ions (especially  $\text{Tb}^{\text{III}}$ ,  $\text{Dy}^{\text{III}}$ , and  $\text{Ho}^{\text{III}}$ ), bring large magnetic moments and high uniaxial magnetic anisotropy, which are essential prerequisites for the observation of slow relaxation of the magnetization. While SMMs can be mono- and oligonuclear (homo- and heteronuclear) complexes, most of the SCMs are constructed from two different spin carriers (e.g., 3d-3d', 3d-4f, 2p-3d, and 2p-4f) [4]. Homospin SCMs are rare and rather serendipitously obtained [5,6]. Examples of lanthanide-based Single-Chain Magnets are also limited, and most of them result from the association of lanthanide ions with nitronyl-nitroxide (paramagnetic) ligands [7,8]. Lanthanide ions can be linked to other paramagnetic metal ions through small bridging ligands, which facilitate the exchange interactions. The building-block approach, relying on the employment of metalloligands, represents an excellent strategy to generate heterometallic coordination compounds [9]. Anionic cyanido complexes are very popular in this respect. The self-assembly processes between  $[\text{M}(\text{CN})_6]^{3-}$  metalloligands and cationic  $\text{Ln}^{\text{III}}$  complexes led to a rich variety of structural architectures. The assembling complex cations are either solvated  $\text{Ln}^{\text{III}}$  species or heteroleptic complexes, containing chelating ligands and weakly coordinated anions or solvent molecules, which can be easily replaced by the cyanido bridge. The dimensionality

of the resulting coordination polymers is dependent on the number of accessible positions at the lanthanide ions. For example, nitrogen donor blocking ligands attached to  $\text{Ln}^{\text{III}}$  ions, such as 1,10-phenanthroline, 2,2'-bipyridine, 2,2':6',2''-terpyridine, 2,4,6-tri(2-pyridyl)-1,3,5-triazine, favor the aggregation of 1D coordination polymers, employing  $[\text{M}(\text{CN})_6]^{3-}$  as metalloligands [10–18]. When the reactions between the lanthanide salts and the hexacyanido building block occur in dimethylformamide (DMF) or dimethyl sulfoxide (DMSO), depending on the experimental conditions, discrete species, 1D, 2D, or even 3D coordination polymers have been obtained [19–24]. By decreasing the number of cyanido groups within the metalloligand, the formation of low-dimensionality coordination polymers is favored [25]. Most of these 3d-4f cyanido-bridged complexes show interesting physical properties, mainly magnetic [26–28] and optical [29–31], and in some cases combined slow magnetic relaxation and light emission were revealed [32,33].

In this paper, we report on a new family of 1D coordination polymers, which are assembled from  $[\text{LnL}]^{3+}$  and  $[\text{M}(\text{CN})_6]^{3-}$  ions ( $\text{L} = \text{bis-semicarbazone ligand}$ ,  $\text{M} = \text{Fe, Co}$ ). The pentadentate *bis-semicarbazone* ligand, **L** (Scheme 1), was previously used for the synthesis of both 3d-3d/3d-4d cyanido-bridged discrete [34] and polymeric structures [35–41].



**Scheme 1.** The structure of *bis-semicarbazone* ligand, **L**.

The new compounds have been characterized by single-crystal X-ray diffraction, and their magnetic properties have been investigated.

## 2. Experimental Section

### 2.1. Materials and Physical Measurements

All reagents and solvents for synthesis were commercially purchased and used without any further purification. The *bis-semicarbazone* ligand **L** was synthesized according to the method reported in the literature [42].

IR spectra were recorded on a FTIR Bruker Tensor V-37 spectrophotometer (KBr pellets) in the range of  $4000\text{--}400\text{ cm}^{-1}$ . Elemental analysis was performed on a EuroEA Elemental Analyzer.

**Magnetic Studies:** DC magnetic susceptibility data (2–300 K) were collected on powdered samples using a SQUID magnetometer (Quantum Design MPMS-XL), applying a magnetic field of 0.1 T. All data were corrected for the contribution of the sample holder and the diamagnetism of the samples estimated from Pascal's constants [43,44]. The field dependence of the magnetization (up to 5 T) was measured between 2.0 and 5.0 K. AC magnetic susceptibility was measured between 2 and 7 K with an oscillating field magnitude of  $H_{\text{ac}} = 3.0\text{ Oe}$  and frequency ranging between 1 and 1488 Hz in presence of a dc field up to  $H_{\text{dc}} = 4000\text{ Oe}$ . Fitting of the variable parameters and estimation of errors was performed with lsqcurvefit solver in MATLAB, and jacobian matrix was used to generate 95% confidence intervals on the fitted parameters. Typical examples of this analysis are presented in Figures S3–S6.

X-ray powder diffraction data were measured on a Proto AXRD benchtop using Cu-K $\alpha$  radiation with a wavelength of  $1.54059\text{ \AA}$  in the range of  $5\text{--}35^\circ$  ( $2\theta$ ).

## 2.2. Single Crystal X-ray Crystallography

X-ray diffraction data were collected at 293 K on a Rigaku XtaLAB Synergy-S diffractometer operating with Mo-K $\alpha$  ( $\lambda = 0.71073 \text{ \AA}$ ) micro-focus sealed X-ray tube. The structures were solved by direct methods and refined by full-matrix least squares techniques based on  $F^2$ . The non-H atoms were refined with anisotropic displacement parameters. Calculations were performed using SHELX-2014 or SHELX-2018 crystallographic software package [45,46]. Supplementary X-ray crystallographic data in CIF format have been deposited with the CCDC with the following reference numbers: 2069217 ( $1_{\text{GdFe}}$ ), 2069215 ( $2_{\text{DyFe}}$ ), and 2069216 ( $3_{\text{DyCo}}$ ). A summary of the crystallographic data and the structure refinement for crystals 1–3 are given in Table S1.

## 2.3. Synthesis of Complexes

The three compounds are synthesized following the same general procedure:  $\text{LnCl}_3 \cdot 6\text{H}_2\text{O}$  (0.06 mmol) and L (0.06 mmol) in 10 mL  $\text{H}_2\text{O}$  were stirred at 80 °C for 30 min. The above-cooled solution was filtered and transferred to a 30 mL test tube. Additional 5 mL of water was layered over the aqueous solution of the mononuclear complexes, and finally, a 10 mL  $\text{H}_2\text{O}$  solution containing 0.06 mmol  $\text{K}_3[\text{Fe}(\text{CN})_6]$  or  $\text{K}_3[\text{Co}(\text{CN})_6]$  was then slowly layered on top. The whole set up was kept undisturbed and slow diffusion of these two solutions led, after 2 weeks, to single crystals. The reaction mixture was mechanically stirred and was filtered off through frit followed by drying under vacuum to obtain a polycrystalline solid. Single crystals required for the X-ray data collections were picked up from the crystalline mixtures prior to mechanical stirring.

$\{[\text{Gd}(\text{L})(\text{H}_2\text{O})_2\text{Fe}(\text{CN})_6] \cdot \text{H}_2\text{O}\}_n$ ,  $1_{\text{GdFe}}$ : Orange crystalline solid, mass (yield): 22 mg (51 %). Selected IR data (KBr,  $\text{cm}^{-1}$ ): 3457 (m), 3349 (m), 3189 (m), 2147 (mw), 2121 (vs), 1677 (vs), 1629 (m), 1614 (m), 1542 (s), 1461 (mw), 1367 (mw), 1307 (mw), 1266 (mw), 1196 (s), 1174 (mw), 1138 (mw), 1106 (mw), 1004 (w), 815 (mw), 769 (mw), 705 (mw), 656 (mw), 563 (mw), 485 (mw), 417 (mw). Elemental analysis. Calcd. for  $\text{C}_{17}\text{H}_{21}\text{N}_{13}\text{O}_5\text{FeGd}$ : C, 29.15; H, 3.02; N, 25.99%; found C, 29.09; H, 2.96; N, 26.01%.

$\{[\text{Dy}(\text{L})(\text{H}_2\text{O})_2\text{Fe}(\text{CN})_6] \cdot 3\text{H}_2\text{O}\}_n$ ,  $2_{\text{DyFe}}$ : Orange crystalline solid, mass (yield): 27 mg (60 %). Selected IR data (KBr,  $\text{cm}^{-1}$ ): 3457 (m), 3348 (w), 3236 (mw), 1676 (m), 1631 (m), 1609 (m), 1542 (m), 1461 (m), 1371 (m), 1309 (s), 1267 (s), 1196 (s), 1136 (vs), 1105 (m), 816 (m), 769 (mw), 704 (m), 654 (mw), 570 (mw), 507 (mw), 487 (mw). Elemental analysis. Calcd. for  $\text{C}_{17}\text{H}_{25}\text{N}_{13}\text{O}_7\text{DyFe}$ : C, 27.53; H, 3.40; N, 24.55%; found C, 27.25; H, 3.37; N, 24.69%.

$\{[\text{Dy}(\text{L})(\text{H}_2\text{O})_2\text{Co}(\text{CN})_6] \cdot \text{H}_2\text{O}\}_n$ ,  $3_{\text{DyCo}}$ : White crystalline solid, mass (yield): 22 mg (51 %). Selected IR data (KBr,  $\text{cm}^{-1}$ ): 3458 (s), 3349 (s), 3238 (s), 3189 (mw), 2917 (mw), 2849 (w), 2362 (mw), 2165 (mw), 2148 (mw), 2132 (vs), 2091 (w), 1677 (vs), 1631 (m), 1614 (m), 1542 (vs), 1464 (m), 1368 (m), 1309 (mw), 1268 (mw), 1199 (ms), 1174 (mw), 1138 (m), 1107 (m), 1005 (w), 816 (mw), 770 (m), 708 (mw), 656 (mw), 556 (mw), 495 (m), 478 (m), 459 (mw), 422 (m). Elemental analysis. Calcd. for  $\text{C}_{17}\text{H}_{21}\text{N}_{13}\text{O}_5\text{CoDy}$ : C, 28.80; H, 2.99; N, 25.69%; found C, 28.64; H, 2.98; N, 25.45%.

## 3. Results and Discussion

### 3.1. Synthesis and Structures of the Complexes

The three compounds,  $\{[\text{Gd}(\text{L})(\text{H}_2\text{O})_2\text{Fe}(\text{CN})_6] \cdot \text{H}_2\text{O}\}_n$ ,  $1_{\text{GdFe}}$ ,  $\{[\text{Dy}(\text{L})(\text{H}_2\text{O})_2\text{Fe}(\text{CN})_6] \cdot 3\text{H}_2\text{O}\}_n$ ,  $2_{\text{DyFe}}$ , and  $\{[\text{Dy}(\text{L})(\text{H}_2\text{O})_2\text{Co}(\text{CN})_6] \cdot \text{H}_2\text{O}\}_n$ ,  $3_{\text{DyCo}}$ , have been obtained via slow diffusion of water solutions containing  $[\text{Ln}(\text{L})(\text{H}_2\text{O})_4]\text{Cl}_3 \cdot \text{K}_3[\text{M}(\text{CN})_6]$  in 1:1 molar ratio. All complexes show C=O and C=N IR absorption peaks in the range of 1654–1657  $\text{cm}^{-1}$ , which indicate the presence of the semicarbazone ligand. The split bands at 2200–2100  $\text{cm}^{-1}$  are assigned to both the monodentate and bridging cyanido groups [47]. The crystalline phase purity of the samples was confirmed by the good agreement between the PXRD patterns and the ones simulated using single-crystal data (Figure S1). The FTIR spectra are displayed in Figure S2.

Complexes  $1_{\text{GdFe}}$  and  $3_{\text{DyCo}}$  are isostructural, and they crystallize in the orthorhombic space group  $Pbca$  with one crystallization water molecule/formula unit. Complex

$2_{\text{DyFe}}$  crystallizes in the monoclinic system, space group  $P2_1/c$ , with three lattice water molecules/formula unit. In all complexes, the metal ions have similar coordination environments, and the topology of the heterometallic chains is identical.

Compounds  $1_{\text{GdFe}}$  and  $3_{\text{DyCo}}$  consist of heterometallic chains with alternating distributions of the 3d and 4f metal ions. Since the two compounds are isostructural, we will describe only the crystal structure of the compound  $1_{\text{GdFe}}$ . The general appearance of the chains is crenel-like, due to the fact that the  $[\text{Fe}(\text{CN})_6]^{3-}$  metalloligand acts as a bridge trough two *cis* cyanido groups and the two neighboring connecting  $[\text{Fe}(\text{CN})_6]^{3-}$  moieties are placed on the same side of the organic ligand coordinated to the lanthanide ion (Figure 1). One of the two water molecules coordinated to the lanthanide ion is involved in intra-chain hydrogen interaction with a cyanido group from a  $[\text{Fe}(\text{CN})_6]^{3-}$  metalloligand coordinated to a neighboring lanthanide ion. The chains are running along the crystallographic *a* axis.

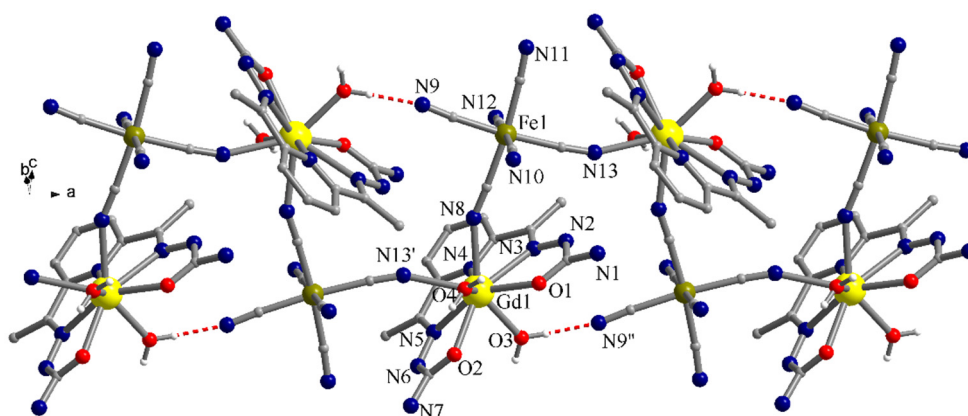


**Figure 1.** Perspective view of the 1D coordination polymer in compound  $1_{\text{GdFe}}$  (symmetry codes:  $' = -0.5 + x, 0.5 - y, 1 - z$ ;  $'' = 0.5 + x, 0.5 - y, 1 - z$ ).

The lanthanide ions are nine-coordinated by the pentadentate organic ligand (O1, O2, N3, N4, and N5), two nitrogen atoms arising from the cyanido bridges (N8, N13'; symmetry code:  $' = -0.5 + x, 0.5 - y, 1 - z$ ), and two aqua ligands (O3, O4). The Ln-N bond lengths with the organic ligand are in the range of 2.584(6) – 2.598(6) Å for  $1_{\text{GdFe}}$  and 2.562(2) – 2.574(2) for  $3_{\text{DyCo}}$ , respectively, while for the cyanido groups are Gd1-N8 = 2.534(6), Gd1-N13' = 2.566(6), respectively, Dy1-N8 = 2.519(3) and Dy1-N13' = 2.544(3). The Ln-O bond lengths are slightly longer with the organic ligand than aqua ligands: Gd1-O1 = 2.423(5), Gd1-O2 = 2.406(5), Gd1-O3 = 2.330(5), Gd1-O4 = 2.375(5), Dy1-O1 = 2.398(2), Dy1-O2 = 2.382(2), Dy1-O3 = 2.308(2), Dy1-O4 = 2.3518(19) Å. The coordination geometry of the gadolinium ion can be described as spherical capped square antiprism, according to the calculations made with SHAPE software (Table S2) [48].

The O3 aqua ligands are further connected by hydrogen bonding to neighboring chains generating a 2D supramolecular architecture in the crystallographic *ac* plane (Figure 2). The distances for the hydrogen interactions are: (O3)H1O...N9'' = 1.85 and (O3)H2O...N11''' = 1.93 Å, while the corresponding angles are: O3-H1O...N9'' = 173.4 and O3-H2O...N11''' = 170.6° (symmetry codes:  $'' = 0.5 + x, 0.5 - y, 1 - z$ ;  $''' = x, 0.5 - y, -0.5 + z$ ).

The extension of the supramolecular architecture to 3D is also mediated by hydrogen bond interactions involving the second aqua ligand, the crystallization water molecules and cyanido groups of the anionic metalloligand (Figure 3). Each O4 coordinated water molecule is involved as donor in hydrogen interactions with two crystallization water molecules. Each crystallization water molecule is acceptor for two hydrogen interactions with two coordinated water molecules from neighboring layers and donor for two cyan groups also from the two neighboring layers. The distances for these hydrogen interactions are: (O4)H4O...O5 = 1.95, (O4)H3O...O5<sup>i</sup> = 1.92, (O5)H5O...N10 = 2.18 and (O5)H6O...N12<sup>ii</sup> = 2.14 Å, while the corresponding angles are: O4-H4O...O5 = 166.7, O4-

$\text{H3O}\cdots\text{O5}^i = 161.8$ ,  $\text{O5-H5O}\cdots\text{N10} = 158.7$  and  $\text{O5-H6O}\cdots\text{N12}^{ii} = 169.7^\circ$  (symmetry codes:  $^i = 1 - x, -y, 1 - z$ ;  $^{ii} = 1.5 - x, -0.5 + y, z$ ).

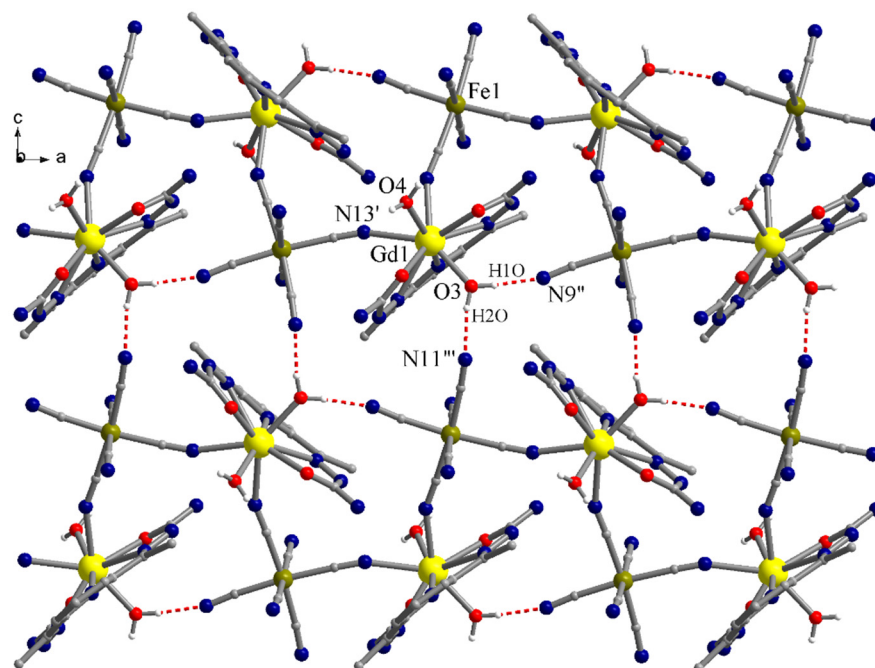


**Figure 2.** View along the crystallographic  $b$  axis of the packing diagram of compound  $1_{\text{GdFe}}$  showing a supramolecular layer (symmetry codes:  $^i = -0.5 + x, 0.5 - y, 1 - z$ ;  $^{ii} = 0.5 + x, 0.5 - y, 1 - z$ ;  $^{iii} = x, 0.5 - y, -0.5 + z$ ).

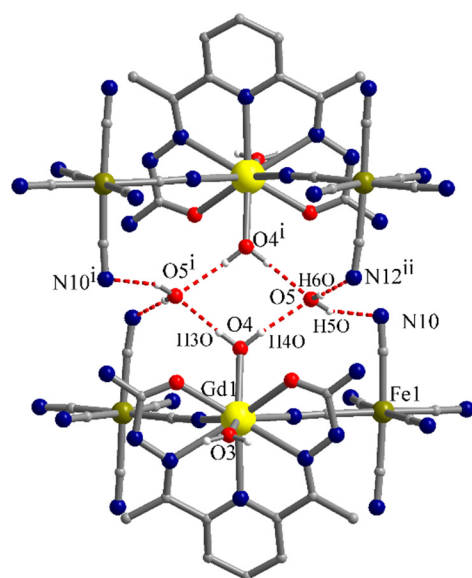


**Figure 3.** Detail of the packing diagram with the hydrogen interactions established between chains from neighboring supramolecular layers and crystallization water molecules in crystal  $1_{\text{GdFe}}$  (symmetry codes:  $^i = 1 - x, -y, 1 - z$ ;  $^{ii} = 1.5 - x, -0.5 + y, z$ ).

Compound  $2_{\text{DyFe}}$  consists also of heterometallic chains running in this case along the crystallographic  $b$  axis, and crystallization water molecules. The 1D chains are formed in a similar manner by connecting  $[\text{Dy}(\text{L})(\text{H}_2\text{O})_2]^{3+}$  complex cations by the  $[\text{Fe}(\text{CN})_6]^{3-}$  metalloligands, which employ two *cis* cyanido groups for bridging (Figure 4). The  $\text{Dy}^{\text{III}}$  ion is nine-coordinated by the pentadentate ligand (O1, O2, N3, N4, and N5), two nitrogen

atoms arising from the cyanido bridges (N8, N13), and two aqua ligands (O3, O4). The coordination geometry of the dysprosium ion is also spherical capped square antiprism (Table S2). The Dy-N and Dy-O bond lengths are in the range of 2.503(2)–2.553(2) and 2.3298(18)–2.3783(13) Å, respectively. The two Dy-N bond distances (nitrogen atoms arising from the bridging cyanido groups) are Dy1-N8 = 2.556(2) and Dy1-N13' = 2.533(2) Å (symmetry code: ' = 1 - x, -0.5 + y, 1.5 - z). The Fe<sup>III</sup> ions show a slightly distorted octahedral geometry with Fe1-C bond lengths ranging from 1.929(3) to 1.957(3) Å. Each {Dy(L)(H<sub>2</sub>O)<sub>2</sub>} module links two {Fe(CN)<sub>6</sub>} fragments in *cis* positions (the Dy...Fe...Dy angle is 95.78°), and each {Fe(CN)<sub>6</sub>} metalloligand connects two Dy<sup>III</sup> ions, resulting in a crenel-like chain structure.

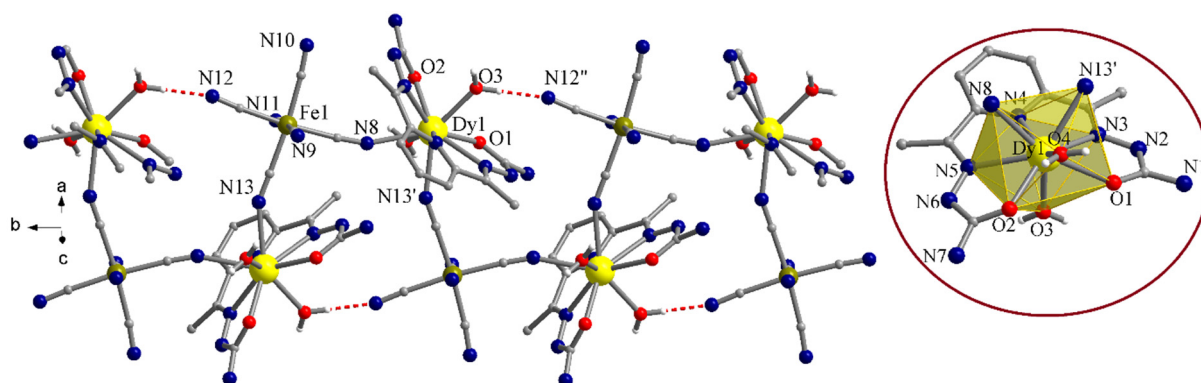


**Figure 4.** Perspective view of the 1D coordination polymer in compound  $2_{DyFe}$ . The inset shows a detail of the coordination environment of the Dy<sup>III</sup> ion (symmetry codes: ' = 1 - x, -0.5 + y, 1.5 - z; '' = x, -1 + y, z).

The O3 aqua ligand is also involved in intra- and interchain hydrogen bonding generating an analogous 2D supramolecular architecture in the *ab* crystallographic plane (Figure 5). The distances for the hydrogen interactions are: (O3)H1O...N12'' = 1.88 and (O3)H2O...N10''' = 2.05 Å, while the corresponding angles are: O3-H1O...N12'' = 172.4 and O3-H2O...N10''' = 167.9° (symmetry codes: '' = x, -1 + y, z; ''' = 2 - x, -0.5 + y, 1.5 - z).

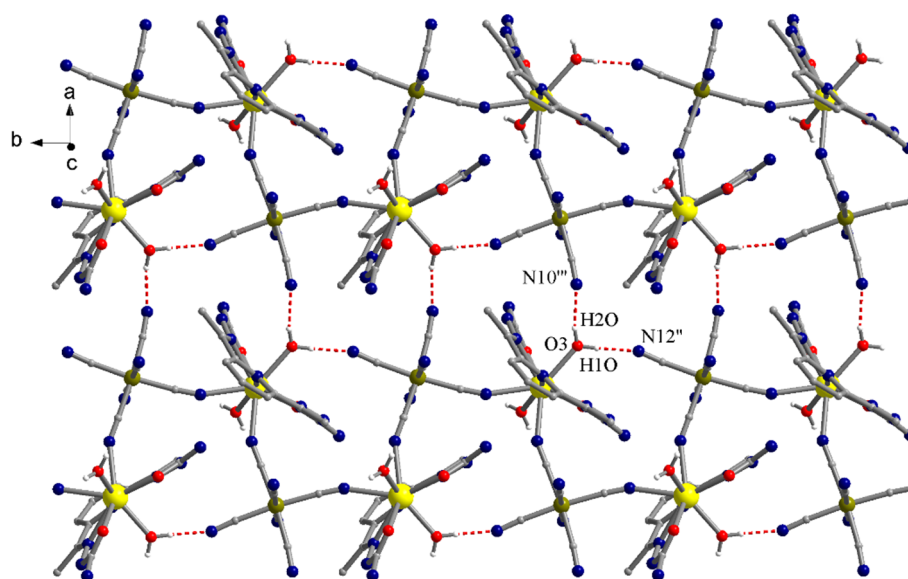


**Figure 5.** View along the crystallographic *c* axis of the packing diagram of compound  $2_{DyFe}$  showing a supramolecular layer (symmetry codes: '' = x, -1 + y, z; ''' = 2 - x, -0.5 + y, 1.5 - z).

The main differences between crystals  $1_{GdFe}$  and  $2_{DyFe}$  appear in hydrogen interactions established between the supramolecular layers. Compound  $2_{DyFe}$  has two more crystal-

lization water molecules per unit comparing with the crystals  $1_{\text{GdFe}}$  and  $3_{\text{DyCo}}$ . The O4 coordinated water molecule is also involved as donor in hydrogen interactions with two crystallization water molecules, O5 and O5<sup>i</sup>, (Figure 6). Each of these crystallization water molecules is acceptor for two hydrogen interactions with two coordinated water molecules from neighboring layers and acts as donor for only one cyanido group (O5 is donor for N11<sup>i</sup> atom). The other two crystallization water molecules are involved in hydrogen bonding with one NH<sub>2</sub> group and one cyanido group (O6), respectively, and two cyanido groups (O7). The distances for the hydrogen interactions are: (O4)H4O...O5 = 1.91, (O4)H3O...O5<sup>i</sup> = 2.02, (O5)H5O...N11<sup>i</sup> = 2.28, (N7)H5N...O6 = 2.16, (O6)H8O...N12<sup>iii</sup> = 2.28, (O7)H9O...N9<sup>ii</sup> = 2.15, and (O7)H10O...N10<sup>i</sup> = 2.20 Å, while the corresponding angles are: O4-H4O...O5 = 174.4, O4-H3O...O5<sup>i</sup> = 171.4, O5-H5O...N11<sup>i</sup> = 146.7, N7-H5N...O6 = 162.3, O6-H8O...N12<sup>iii</sup> = 166.1, O7-H9O...N9<sup>ii</sup> = 153.9, and O7-H10O...N10<sup>i</sup> = 148.8 ° (symmetry codes: <sup>i</sup> = 1 - x, 1 - y, 1 - z; <sup>ii</sup> = 1 - x, -0.5 + y, 1.5 - z; <sup>iii</sup> = x, 1.5 - y, -0.5 + z).

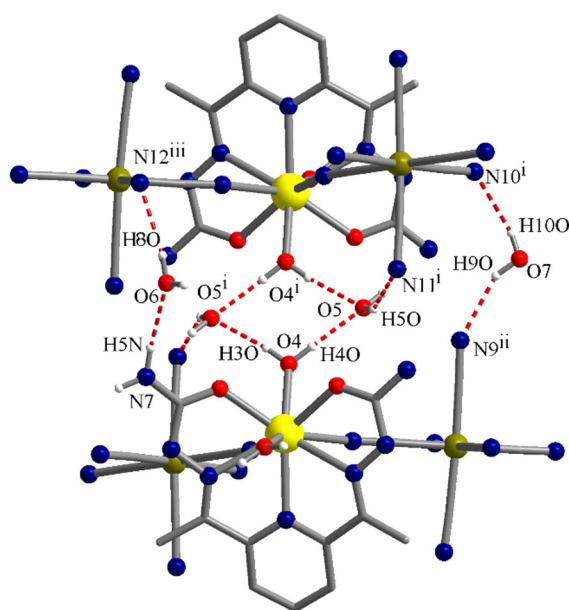


**Figure 6.** Detail of the packing diagram with the hydrogen interactions established between chains from neighboring supramolecular layers and crystallization water molecules in crystal  $2_{\text{DyFe}}$  (symmetry codes: <sup>i</sup> = 1 - x, 1 - y, 1 - z; <sup>ii</sup> = 1 - x, -0.5 + y, 1.5 - z; <sup>iii</sup> = x, 1.5 - y, -0.5 + z).

The shortest intramolecular Fe...Gd distances in  $1_{\text{GdFe}}$  are 5.513 and 5.557 Å, while the intramolecular Dy...Fe distances in  $2_{\text{DyFe}}$  are 5.542 and 5.494 Å. Selected bond distances and angles for compounds **1–3** are listed in Table S3.

### 3.2. Magnetic Properties of the Complexes

**Static magnetic characterizations.** The magnetic susceptibility data for compounds **1–3** were measured on polycrystalline samples in the temperature range of 2–300 K as shown in Figure 7, in the form of  $\chi_{\text{M}}T$  vs.  $T$  curves. The observed  $\chi_{\text{M}}T$  values at 300 K for  $1_{\text{GdFe}}$ ,  $3_{\text{DyCo}}$ , and  $2_{\text{DyFe}}$  are of 8.265, 15.454, and 16.305 cm<sup>3</sup> mol<sup>-1</sup> K, which are slightly higher than the expected values for a non-interacting spin system of one Gd<sup>III</sup> (7.88 cm<sup>3</sup> mol<sup>-1</sup> K,  $S = 7/2$ ,  $^8\text{S}_{7/5}$ ,  $g = 2.00$ ), Dy<sup>III</sup> (14.17 cm<sup>3</sup> mol<sup>-1</sup> K,  $S = 5/2$ ,  $^6\text{H}_{15/2}$ ,  $g = 4/3$ ) [49], and one low-spin  $S = \frac{1}{2}$  Fe<sup>III</sup> ion or one diamagnetic Co<sup>III</sup> ion [44]. Upon cooling, the  $\chi_{\text{M}}T$  values stay almost constant in the high temperature region, while at low temperatures, the  $\chi_{\text{M}}T$  values show a rapid decrease and reach the values of 6.833, 12.722, and 11.210 cm<sup>3</sup> mol<sup>-1</sup> K, respectively, at 2.0 K. In the case of  $1_{\text{GdFe}}$ , the decrease in  $\chi_{\text{M}}T$  with temperature may be associated with Fe<sup>III</sup>-Gd<sup>III</sup> antiferromagnetic interactions along the heterometallic alternating chain. The possible presence of intermolecular interactions can also contribute to this decrease. The expected ferrimagnetic behavior (i.e., the characteristic minimum on the

$\chi_M T$  vs.  $T$  curve) is not observed, probably due to the small magnitude of the exchange interactions along the chain. The evolution of the temperature dependence of the magnetic susceptibility for  $3_{\text{DyCo}}$  is exclusively defined by the presence of strongly anisotropic  $\text{Dy}^{\text{III}}$  ions, which are isolated by diamagnetic low spin  $\text{Co}^{\text{III}}$  ions. The decrease in  $\chi_M T$  with the temperature is due to the depopulation of  $M_J$  (Stark) sublevels of the  $\text{Dy}^{\text{III}}$  centers in  $3_{\text{DyCo}}$  [50]. This effect is certainly present in the case of compound  $2_{\text{DyFe}}$ . Additionally, a  $\text{Fe}^{\text{III}}\text{-Dy}^{\text{III}}$  magnetic coupling along the chain can be expected. In the case of  $2_{\text{DyFe}}$ , the evolution of  $\chi_M T$  shows a more important slope compared to compound  $3_{\text{DyCo}}$  (Figure 7), with a lower value of susceptibility at 2.0 K ( $11.210 \text{ cm}^3 \text{ mol}^{-1} \text{ K}$ ). This indicates the presence of some antiferromagnetic impact, which contributes to the observed decreasing  $\chi_M T$  values. For  $2_{\text{DyFe}}$ , the existence of magnetic interactions similar to those in  $1_{\text{GdFe}}$  also suggests the formation of a ferrimagnetic chain, which, associated with strong magnetic anisotropy, could lead to a Single Chain Magnet. Unfortunately, as in the case of  $1_{\text{GdFe}}$ , the increase in  $\chi_M T$  at low temperatures and the characteristic minimum were not detected for  $2_{\text{DyFe}}$  (Figure 7). This behavior is probably due to the very small antiferromagnetic interactions along the chain. The magnetization measurements (Figure S3) support the presence of an important magnetic anisotropy in  $2_{\text{DyFe}}$  and  $3_{\text{DyCo}}$ .

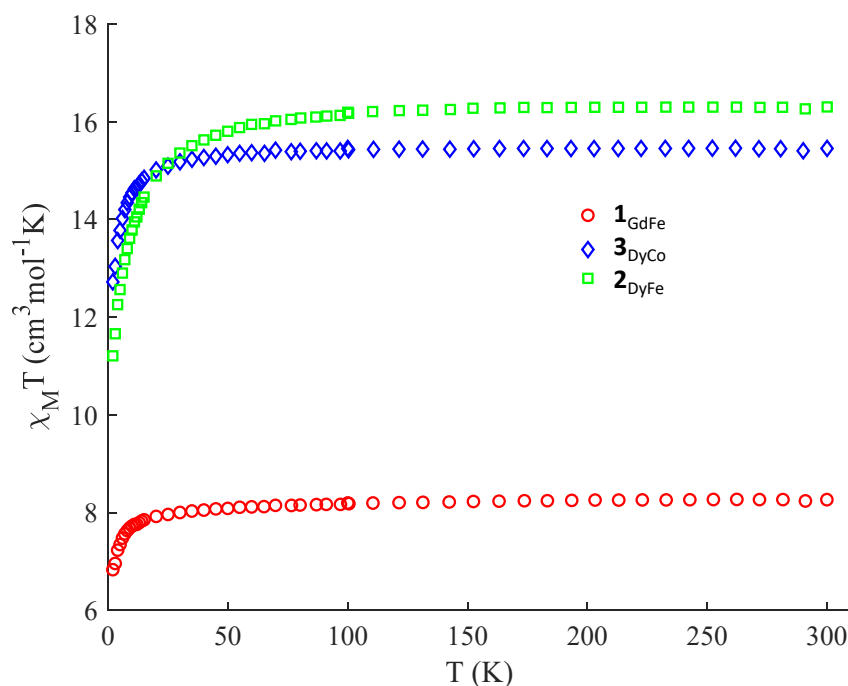


**Figure 7.** Temperature dependence of  $\chi_M T$  vs.  $T$  for complexes  $1_{\text{GdFe}}$ ,  $2_{\text{DyFe}}$ , and  $3_{\text{DyCo}}$ .

**Dynamic magnetic characterizations.** Dynamic magnetic properties of the compounds  $1_{\text{GdFe}}$ ,  $2_{\text{DyFe}}$ , and  $3_{\text{DyCo}}$  were studied by measuring the temperature and field dependence *ac* (alternative current) magnetic susceptibility. Compound  $1_{\text{GdFe}}$  does not have any manifestation of the out-of-phase component ( $\chi''_{ac}$ ) of the *ac* magnetic susceptibility at 2 K and zero *dc* (direct current) field. After applying small *dc* field (2000 Oe) no modification was observed in  $\chi''_{ac}$  component of *ac* susceptibility.

For  $3_{\text{DyCo}}$ , no signal was observed under zero *dc* field at 2.0 K, in  $\chi''_{ac}$  component of *ac* susceptibility. After applying of small *dc* fields (up to 4000 Oe), a frequency dependent out-of-phase signal appears (Figure 8b) and has a rich evolution in function of the field. Such behavior is consistent with presence of strongly anisotropic paramagnetic centers  $\text{Dy}^{\text{III}}$  and indicates the presence of field-induced slow magnetic relaxation. The intensity of the out-of-phase signals gradually increases till about 2000 Oe, and then, it slightly decreases. To investigate the nature of slow magnetic relaxation, additional *ac* susceptibility data were

collected under fixed  $dc$  field (2000 Oe) and stable temperatures between 2.0 and 5.0 K (with a 0.2 K increment)—Figure 8d–f. The temperature sweeping of the  $ac$  susceptibility shows the important evolution of the  $\chi''_{ac}$  component and supports the presence of field-induced slow magnetic relaxation in  $3_{DyCo}$ . Since the  $Co^{III}$  ion is diamagnetic, compound  $3_{DyCo}$  can be described as being a chain of Single Ion Magnets.

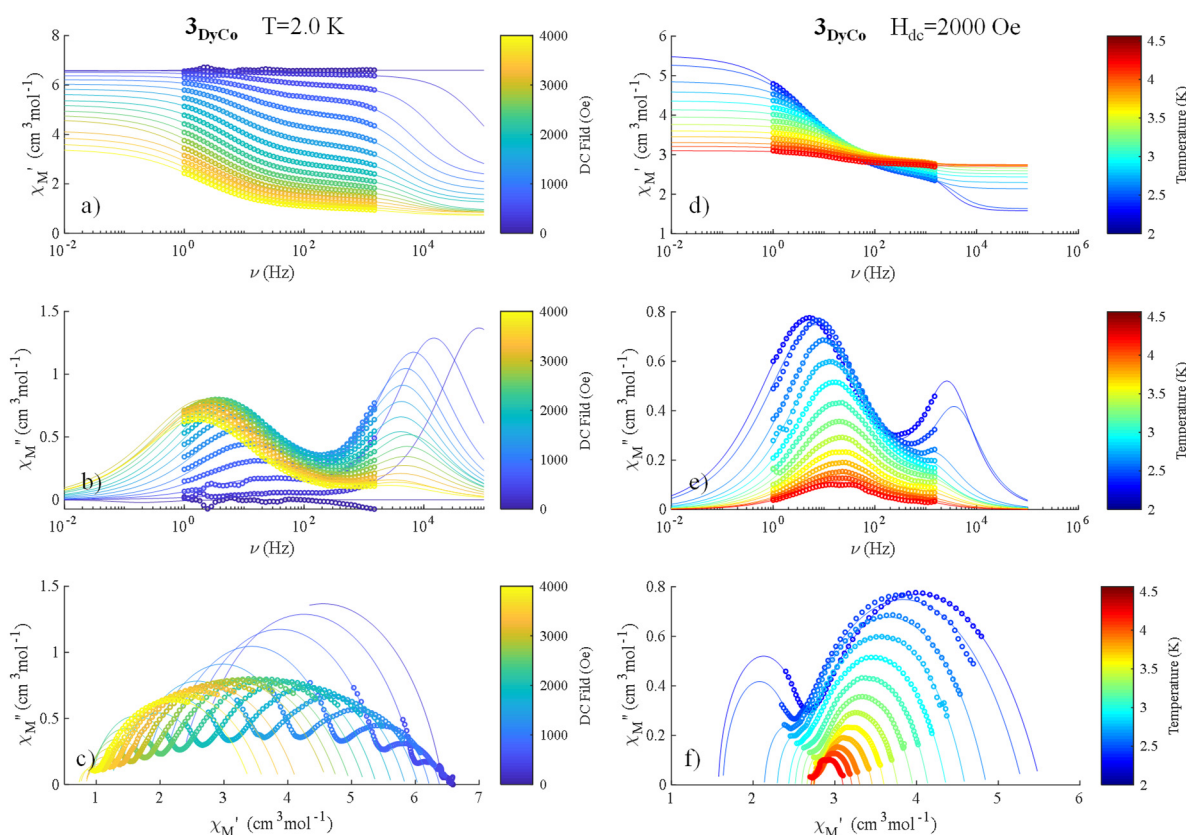


**Figure 8.** Field dependence (left, a,b) and temperature dependence (right, d,e) of  $ac$  susceptibility ( $H_{ac} = 3.0$  Oe) and Cole–Cole plots, (c,f), for  $3_{DyCo}$  at the indicated temperatures and fields. The solid lines represent the best fits according to the generalized Debye model for two relaxations processes (Equations (S1) and (S2)).

A similar strategy of measurements was used in the dynamic analysis of  $2_{DyFe}$ . As in the case of  $3_{DyCo}$ , at  $T = 2.0$  K and zero  $dc$  field, no signal was detected in the out-of-phase component of the  $ac$  susceptibility. The signals appear when a small magnetic  $dc$  field was applied and has similar evolutions as in the case of  $3_{DyCo}$  (Figure S8a–c). A  $dc$  field of 3000 Oe was used to perform the temperature sweeping measurements of the  $ac$  susceptibility in the case of  $2_{DyFe}$  (Figure S8d–f).

For both compounds ( $2_{DyFe}$  and  $3_{DyCo}$ ), the visual analysis of the out-of-phase susceptibilities, as well of the  $\chi''_{ac}$  vs.  $\chi'_{ac}$  plots (Cole–Cole plots), suggests the presence of at least two distinct relaxation processes. In consequence, the  $ac$  susceptibility data (field sweeping and temperature sweeping measurements) for  $3_{DyCo}$  and  $2_{DyFe}$  were evaluated with generalized (extended) Debye equations combining two-relaxation processes [51–53]. The two relaxation times ( $\tau_1$ , and  $\tau_2$ ) and two distribution parameters ( $\alpha_1$ , and  $\alpha_2$ ) occur along with two isothermal susceptibilities ( $\chi_{T1}$  and  $\chi_{T2}$ ) and one common adiabatic susceptibility ( $\chi_s$ ) (see Equations (S1) and (S2)). The deconvolution of two relaxations process is presented in Figures S4–S7. Variable parameters derived from the best fits of the  $ac$  susceptibility are shown in Figures S9–S12.

In both compounds, the first relaxation process LF (Low Frequency) is well defined, while the second HF (High Frequency) process has large errors on the variable parameters. The distributions of relaxation times for the LF process are rather broad ( $\alpha_1 = 0.3 \div 0.5$ ). The

extracted temperature and field dependence of relaxation times for  $2_{\text{DyFe}}$  and  $3_{\text{DyCo}}$  can be modulated based on four relaxation mechanisms according to the following equation [54–58]:

$$\tau_{T/H}^{-1}(T, H) = \frac{Q_1}{1 + Q_2 H^2} + \tau_0^{-1} \exp\left(-\frac{U_{\text{eff}}}{kT}\right) + AH^4 T + CT^n. \quad (1)$$

The first term represents the Quantum Tunneling of Magnetization (QTM), the second term corresponds to Orbach, the third to Direct, and the last one to Raman process; moreover,  $H$  = applied *dc* magnetic field and  $T$  = temperature. In order to constrain the variable parameters and avoid the overparameterization problem, temperature and field dependence of relaxation times were fitted simultaneously [56] (vector of data:  $\tau^{-1}$  in  $\text{s}^{-1}$ ,  $T$  in Kelvin, and  $H$  in kOe). Only LF signals will be discussed below, as the second process (HF) is poorly defined. Different combinations of the four mechanisms of relaxation have been used in order to simulate the evolution of the relaxation times. For the LF signals, with both compounds, the contribution of Quantum Tunneling of Magnetization (QTM) is indispensable to simulate the relaxation data. The continuous decreasing trend of  $\tau^{-1}$  vs. applied field ( $H$ ) excludes the presence of significant contribution of Direct relaxation mechanism. The other contributions in relaxation times can be Raman and/or Orbach, which have the same increasing evolutions with temperature variation [57]. In this restricted range of temperature, it is difficult to separate these two components. In order to have some information regarding the manifestation of these mechanisms, the comparative fits on the temperature dependence of relaxation time for  $2_{\text{DyFe}}$  and  $3_{\text{DyCo}}$  have been done (Figures S13–S15). Both mechanisms can reproduce the time of evolution. The quality of the Orbach mechanism is slightly better. It should be mention here that the distribution parameters ( $\alpha$ ) have important impact on uncertainties relaxation time [59] and can also be an argument in favor of one or another mechanism. The analysis presented in Figures S13–S15 shows the similarity in uncertainties of relaxation times for both mechanisms. Based on this argument and a low temperature range (2–4 K) of relaxation data for  $3_{\text{DyCo}}$  and  $2_{\text{DyFe}}$ , as well the traditional representation of relaxation phenomena in SMM, our analysis of LF relaxation process is limited to two contributions: QTM and Orbach. The best fit for LF relaxation processes based on the two mechanisms has been obtained for the following sets of parameters:

$$3_{\text{DyCo}}: U_{\text{eff}}/k = 7.1 \text{ K}; \tau_0 = 7.5 \times 10^{-5} \text{ s}; Q_1 = 121 \text{ s}^{-1}; Q_2 = 1.05 \text{ kOe}^{-2}$$

$$2_{\text{DyFe}}: U_{\text{eff}}/k = 10.8 \text{ K}; \tau_0 = 5.9 \times 10^{-4} \text{ s}; Q_1 = 200 \text{ s}^{-1}; Q_2 = 0.05 \text{ kOe}^{-2}.$$

The obtained relaxation parameters are similar for compounds  $2_{\text{DyFe}}$  and  $3_{\text{DyCo}}$ . Due to the diamagnetic  $\text{Co}^{\text{III}}$  ions in  $3_{\text{DyCo}}$ , the slow magnetic relaxation is solely associated with the anisotropic  $\text{Dy}^{\text{III}}$  ions. The existence of intrachain magnetic interaction in  $2_{\text{DyFe}}$  does not change significantly the energy barrier of slow relaxation of the magnetization (see the temperature dependence in Figure 9), but affects more the field dependence, which becomes much more redistributed. This probably can be associated to redistribution/mixing the different energy levels in the  $2_{\text{DyFe}}$  as a result of the small antiferromagnetic interaction along the chain and of intermolecular (interchain) interaction. The splitting of  $M_J$  (Stark) sublevels of the  $\text{Dy}^{\text{III}}$  centers under variation of the magnetic field also contributes to this redistribution. As in the case of static magnetic measurements, these competitive interactions cannot be quantified at the reported range of temperatures.

In a recent paper, Ma et al. report on a family of discrete, tetranuclear 3d-4f complexes assembled from a cationic lanthanide complexes and  $[\text{M}(\text{CN})_6]^{3-}$  metalloligands ( $M = \text{Fe}, \text{Co}$ ), the ligand attached to the lanthanide(III) ions (Tb, Dy, and Ho) being also pentadentate [60]. The field-induced slow relaxation of the magnetization, with a low energy barrier (11.17 K), was observed only with the  $[\text{Dy}_2\text{Co}_2]$  derivative. The presence of the paramagnetic  $\text{Fe}^{\text{III}}$  ion does not improve the SMM behavior: for the  $[\text{Dy}_2\text{Fe}_2]$  derivative, the slow relaxation is not observed even by applying *dc* fields.

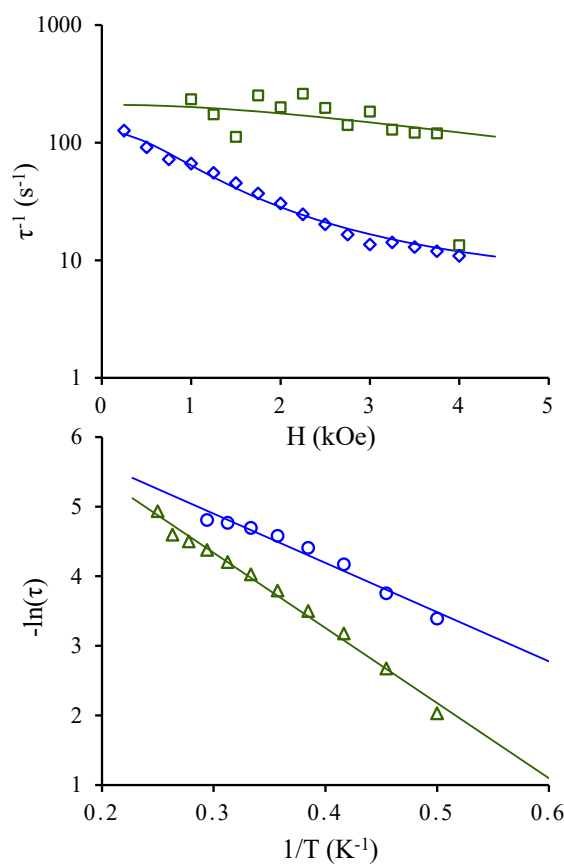


**Figure 9.** Field (up) and temperature (down) dependence of relaxation times for  $3_{\text{DyCo}}$  and  $2_{\text{DyFe}}$ . The solid lines correspond to the fit using QTM and Orbach mechanisms for the magnetic relaxation.

#### 4. Conclusions

In this paper, we have shown that the pentadentate *bis*-semicarbazone ligand, L, generates robust cationic  $\text{Ln}^{\text{III}}$  complexes, which are useful modules for constructing heterometallic coordination polymers. The metalloligands,  $[\text{M}(\text{CN})_6]^{3-}$ , employ two *cis* cyanido groups as bridges against the  $\text{Ln}^{\text{III}}$  ions, resulting in a wave-like chain topology for the three compounds. The investigation of the magnetic properties reveals that the two  $\text{Dy}^{\text{III}}$ -containing coordination polymers exhibit slow relaxation of the magnetization, with rather low energy barriers. From the magnetic point of view, compound  $3_{\text{DyCo}}$  behaves like a chain of Single Ion Magnets. These results open interesting perspectives for the synthesis of new cyanido-bridged 3d-4f complexes, using not only homoleptic but also heteroleptic cyanido tectons, as well as other types of metalloligands. Further work is in progress in our laboratory.

**Supplementary Materials:** The following are available online at <https://www.mdpi.com/article/10.3390/magnetochemistry7050057/s1>, Crystallographic data (single crystal and PXRD), bond distances and angles, infrared spectra; magnetic data; treatment of the ac magnetic data.

**Author Contributions:** Conceptualization, D.D. and M.A.; methodology, M.A., D.D. and G.N.; formal analysis, G.N. and A.M.M.; investigation, D.D., A.M.M. and G.N.; writing—original draft preparation, D.D. and M.A.; writing—review and editing, M.A. and G.N. All authors have read and agreed to the published version of the manuscript.

**Funding:** MAGMOLMET, grant ID: 867445.

**Acknowledgments:** D.D. is grateful to the European Union's Horizon 2020 research and innovation programme, for financial support (MAGMOLMET, grant ID: 867445).

**Conflicts of Interest:** The authors declare no conflict of interest.

## References

1. Woodruff, D.N.; Winpenny, R.E.P.; Layfield, R.A. Lanthanide Single-Molecule Magnets. *Chem. Rev.* **2013**, *113*, 5110–5148. [[CrossRef](#)]
2. Goodwin, C.A.P.; Ortu, F.; Reta, D.; Chilton, N.F.; Mills, D.P. Molecular magnetic hysteresis at 60 Kelvin in dysprosocenium. *Nature* **2017**, *548*, 439–442. [[CrossRef](#)]
3. Guo, F.S.; Day, B.M.; Chen, Y.C.; Tong, M.L.; Mansikkamaki, A.; Layfield, R.A. Magnetic hysteresis up to 80 kelvin in a dysprosium metallocene single-molecule magnet. *Science* **2018**, *362*, 1400–1403. [[CrossRef](#)]
4. Dhers, S.; Feltham, H.L.C.; Brooke, S. A toolbox of building blocks, linkers and crystallisation methods used to generate single-chain magnets. *Coord. Chem. Rev.* **2015**, *296*, 24–44. [[CrossRef](#)]
5. Zheng, Y.-Z.; Lan, Y.; Wernsdorfer, W.; Anson, C.E.; Powell, A.K. Polymerisation of the Dysprosium Acetate Dimer Switches on Single-Chain Magnetism. *Chem. Eur. J.* **2009**, *15*, 12566–12570. [[CrossRef](#)] [[PubMed](#)]
6. Liu, Z.-Y.; Xia, Y.-F.; Jiao, J.; Yang, E.-C.; Zhao, X.-J. Two water-bridged cobalt(ii) chains with isomeric naphthoate spacers: From metamagnetic to single-chain magnetic behaviour. *Dalton Trans.* **2015**, *44*, 19927–19934. [[CrossRef](#)] [[PubMed](#)]
7. Bogani, L.; Sangregorio, C.; Sessoli, R.; Gatteschi, D. Molecular engineering for single-chain-magnet behavior in a one-dimensional dysprosium–nitronyl nitroxide compound. *Angew. Chem. Int. Ed.* **2005**, *44*, 5817–5821. [[CrossRef](#)] [[PubMed](#)]
8. Bernot, K.; Bogani, L.; Caneschi, A.; Gatteschi, D.; Sessoli, R. A family of rare-earth-based single chain magnets: Playing with anisotropy. *J. Am. Chem. Soc.* **2006**, *128*, 7947–7956. [[CrossRef](#)]
9. Pedersen, K.S.; Bendix, J.; Clérac, R. Single-molecule magnet engineering: Building-block approaches. *Chem. Commun.* **2014**, *50*, 4396–4415. [[CrossRef](#)]
10. Pal, S.; Dey, K.; Benmansour, S.; Gómez-García, C.J.; Nayek, H.P. Syntheses, structures and magnetic properties of cyano-bridged one-dimensional Ln<sup>3+</sup>–Fe<sup>3+</sup> (Ln = La, Dy, Ho and Yb) coordination polymers. *New J. Chem.* **2019**, *43*, 6228–6233. [[CrossRef](#)]
11. Yu, D.-Y.; Li, L.; Zhou, H.; Yuan, A.-H.; Li, Y.-Z. Cyano-Bridged 4f-3d Assemblies with Achiral Helical Chains: Syntheses, Structures, and Magnetic Properties. *Eur. J. Inorg. Chem.* **2012**, 3394–3397. [[CrossRef](#)]
12. Estrader, M.; Ribas, J.; Tangoulis, V.; Solans, X.; Font-Bardía, M.; Maestro, M.; Diaz, C. Synthesis, Crystal Structure, and Magnetic Studies of One-Dimensional Cyano-Bridged Ln<sup>3+</sup>–Cr<sup>3+</sup> Complexes with bpy as a Blocking Ligand. *Inorg. Chem.* **2006**, *45*, 8239–8250. [[CrossRef](#)] [[PubMed](#)]
13. Figuerola, A.; Ribas, J.; Casanova, D.; Maestro, M.; Alvarez, S.; Diaz, C. Magnetism of Cyano-Bridged Ln<sup>3+</sup>–M<sup>3+</sup> Complexes. Part II: One-Dimensional Complexes (Ln<sup>3+</sup> = Eu, Tb, Dy, Ho, Er, Tm; M<sup>3+</sup> = Fe or Co) with bpy as Blocking Ligand. *Inorg. Chem.* **2005**, *44*, 6949–6958. [[CrossRef](#)] [[PubMed](#)]
14. Figuerola, A.; Diaz, C.; Ribas, J.; Tangoulis, V.; Sangregorio, C.; Gatteschi, D.; Maestro, M.; Mahía, J. Magnetism of Cyano-Bridged Hetero-One-Dimensional Ln<sup>3+</sup>–M<sup>3+</sup> Complexes (Ln<sup>3+</sup> = Sm, Gd, Yb; M<sup>3+</sup> = FeLS, Co). *Inorg. Chem.* **2003**, *42*, 5274–5281. [[CrossRef](#)] [[PubMed](#)]
15. Petrosyants, S.P.; Ilyukhin, A.B.; Efimov, N.N.; Gavrikov, A.V.; Novotortsev, V.M. Self-assembly and SMM properties of lanthanide cyanocobaltate chain complexes with terpyridine as blocking ligand. *Inorg. Chim. Acta* **2018**, *482*, 813–820. [[CrossRef](#)]
16. Muddassir, M.; Song, X.-J.; Chen, Y.; Cao, F.; Weia, R.-M.; Song, Y. Ion-induced diversity in structure and magnetic properties of hexacyanometalate–lanthanide bimetallic assemblies. *CrystEngComm.* **2013**, *15*, 10541–10549. [[CrossRef](#)]
17. Figuerola, A.; Ribas, J.; Solans, X.; Font-Bardía, M.; Maestro, M.; Diaz, C. One Dimensional 3d–4f Heterometallic Compounds: Synthesis, Structure and Magnetic Properties. *Eur. J. Inorg. Chem.* **2006**, 1846–1852. [[CrossRef](#)]
18. Zhao, H.; Lopez, N.; Prosvirin, A.; Chifotidesa, H.T.; Dunbar, K.R. Lanthanide–3d cyanometalate chains Ln(III)–M(III) (Ln = Pr, Nd, Sm, Eu, Gd, Tb; M = Fe) with the tridentate ligand 2,4,6-tri(2-pyridyl)-1,3,5-triazine (tptz): Evidence of ferromagnetic interactions for the Sm(III)–M(III) compounds (M = Fe, Cr). *Dalton Trans.* **2007**, 878–888. [[CrossRef](#)]
19. Liu, J.; Knoepfel, D.W.; Liu, S.; Meyers, E.A.; Shore, S.G. Cyanide-Bridged Lanthanide(III)–Transition Metal Extended Arrays: Interconversion of One-Dimensional Arrays from Single-Strand (Type A) to Double-Strand (Type B) Structures. Complexes of a New Type of Single-Strand Array (Type C). *Inorg. Chem.* **2001**, *40*, 2842–2850. [[CrossRef](#)]
20. Kou, H.-Z.; Gao, S.; Sun, B.-W.; Zhang, J. Metamagnetism of the First Cyano-Bridged Two-Dimensional Brick-Wall-like 4f–3d Array. *Chem. Mater.* **2001**, *13*, 1431–1433. [[CrossRef](#)]
21. Wilson, D.C.; Liu, S.; Chen, X.; Meyers, E.A.; Bao, X.; Prosvirin, A.V.; Dunbar, K.R.; Hadad, C.M.; Shore, S.G. Water-Free Rare Earth-Prussian Blue Type Analogues: Synthesis, Structure, Computational Analysis, and Magnetic Data of {LnIII(DMF)<sub>6</sub>FeIII(CN)<sub>6</sub>}<sub>∞</sub> (Ln = Rare Earths Excluding Pm). *Inorg. Chem.* **2009**, *48*, 5725–5735. [[CrossRef](#)]
22. Chen, W.-T.; Guo, G.-C.; Wang, M.-S.; Xu, G.; Cai, L.-Z.; Akitsu, T.; Akita-Tanaka, M.; Matsushita, A.; Huang, J.-S. Self-Assembly and Characterization of Cyano-Bridged Bimetallic [Ln–Fe] and [Ln–Co] Complexes (Ln = La, Pr, Nd and Sm). Nature of the Magnetic Interactions between the Ln<sup>3+</sup> and Fe<sup>3+</sup> Ions. *Inorg. Chem.* **2007**, *46*, 2105–2114. [[CrossRef](#)]
23. Chen, W.-T.; Wu, A.-Q.; Guo, G.-C.; Wang, M.-S.; Cai, L.-Z.; Huang, J.-S. Cyano-Bridged 2D Bimetallic 4f–3d Arrays with Monolayered Stair-Like, Brick-Wall-Like, or Bilayered Topologies—Rational Syntheses and Crystal Structures. *Eur. J. Inorg. Chem.* **2010**, 2826–2835. [[CrossRef](#)]
24. Xin, Y.; Wang, J.; Zychowicz, M.; Zakrzewski, J.J.; Nakabayashi, K.; Sieklucka, B.; Chorazy, S.; Ohkosh, S. Dehydration–Hydration Switching of Single-Molecule Magnet Behavior and Visible Photoluminescence in a Cyanido-Bridged DyIII/CoIII Framework. *J. Am. Chem. Soc.* **2019**, *141*, 18211–18220. [[CrossRef](#)]
25. Visinescu, D.; Toma, L.M.; Fabelo, O.; Ruiz-Pérez, C.; Lloret, F.; Julve, M. Low-Dimensional 3d–4f Complexes Assembled by Low-Spin [FeIII(phen)(CN)<sub>4</sub>]<sup>–</sup> Anions. *Inorg. Chem.* **2013**, *52*, 1525–1537. [[CrossRef](#)] [[PubMed](#)]

26. Chorazy, S.; Rams, M.; Wyczesany, M.; Nakabayashi, K.; Ohkoshi, S.; Sieklucka, B. Antiferromagnetic exchange and long-range magnetic ordering in supramolecular networks constructed of hexacyanido-bridged LnIII(3-pyridone)–CrIII (Ln = Gd, Tb) chains. *CrystEngComm*. **2018**, *20*, 1271–1281. [[CrossRef](#)]
27. Xue, A.-Q.; Liu, Y.-Y.; Li, J.-X.; Zhang, Y.; Meng, Y.-S.; Zhu, W.-H.; Zhang, Y.-Q.; Sun, H.-L.; Wang, F.; Qiu, G.-X.; et al. The differential magnetic relaxation behaviours of slightly distorted triangular dodecahedral dysprosium analogues in a type of cyano-bridged 3d–4f zig-zag chain compounds. *Dalton Trans.* **2020**, *49*, 6867–6875. [[CrossRef](#)] [[PubMed](#)]
28. Petrosyants, S.P.; Ilyukhin, A.B.; Efimov, N.N.; Novotortsev, V.M. Cyano-Bridged d–f Ensembles of the Dysprosium Tetrapyridine Complexes with the Hexacyanoferrate Anion. *Russ. J. Coord. Chem.* **2018**, *44*, 660–666. [[CrossRef](#)]
29. Chorazy, S.; Zakrzewski, J.J.; Wang, J.; Ohkoshi, S.; Sieklucka, B. Incorporation of hexacyanidoferrate(III) ion in photoluminescent trimetallic Eu(3-pyridone)[Co1–xFex(CN)6] chains exhibiting tunable visible light absorption and emission properties. *CrystEngComm* **2018**, *20*, 5695–5706. [[CrossRef](#)]
30. Chorazy, S.; Kumar, K.; Nakabayashi, K.; Sieklucka, B.; Ohkoshi, S. Fine Tuning of Multicolored Photoluminescence in Crystalline Magnetic Materials Constructed of Trimetallic EuxTb1–x[Co(CN)6] Cyanido-Bridged Chains. *Inorg. Chem.* **2017**, *56*, 5239–5252. [[CrossRef](#)]
31. Chorazy, S.; Wyczesany, M.; Sieklucka, B. Lanthanide Photoluminescence in Heterometallic Polycyanidometallate-Based Coordination Networks. *Molecules* **2017**, *22*, 1902. [[CrossRef](#)]
32. Chorazy, S.; Rams, M.; Nakabayashi, K.; Sieklucka, B.; Ohkoshi, S. White Light Emissive DyIII Single-Molecule Magnets Sensitized by Diamagnetic [CoIII(CN)6]3– Linkers. *Chem. Eur. J.* **2016**, *22*, 7371–7375. [[CrossRef](#)]
33. Chorazy, S.; Rams, M.; Wang, J.; Sieklucka, B.; Ohkoshi, S. Octahedral Yb(III) complexes embedded in [CoIII(CN)6]-bridged coordination chains: Combining sensitized near-infrared fluorescence with slow magnetic relaxation. *Dalton Trans.* **2017**, *46*, 13668–13672. [[CrossRef](#)]
34. Qian, K.; Huang, X.-C.; Zhou, C.; You, X.-Z.; Wang, X.-Y.; Dunbar, K.R. A Single-Molecule Magnet Based on Heptacyanomolybdate with the Highest Energy Barrier for a Cyanide Compound. *J. Am. Chem. Soc.* **2013**, *135*, 13302–13305. [[CrossRef](#)]
35. Sasnovskaya, V.D.; Kopotkov, V.A.; Talantsev, A.D.; Morgunov, R.B.; Yagubskii, E.B.; Simonov, S.V.; Zorina, L.V.; Mironov, V.S. Synthesis, Structure, and Magnetic Properties of 1D {[MnIII(CN)6][MnII(dapsc)]}n Coordination Polymers: Origin of Unconventional Single-Chain Magnet Behavior. *Inorg. Chem.* **2017**, *56*, 8926–8943. [[CrossRef](#)]
36. Zorina, L.V.; Simonov, S.V.; Sasnovskaya, V.D.; Talantsev, A.D.; Morgunov, R.B.; Mironov, V.S.; Yagubskii, E.B. Slow Magnetic Relaxation, Antiferromagnetic Ordering, and Metamagnetism in MnII(H2dapsc)-FeIII(CN)6 Chain Complex with Highly Anisotropic Fe-CN-Mn Spin Coupling. *Chem. Eur. J.* **2019**, *25*, 14583–14597. [[CrossRef](#)]
37. Bar, A.K.; Gogoi, N.; Pichon, C.; Goli, V.M.L.D.P.; Thlijeni, M.; Duhayon, C.; Suaud, N.; Guihéry, N.; Barra, A.-L.; Ramasesha, S.; et al. Pentagonal Bipyramid FeII Complexes: Robust Ising-spin Units Towards Heteropolynuclear Nano-Magnets. *Chem. Eur. J.* **2017**, *23*, 4380–4396. [[CrossRef](#)] [[PubMed](#)]
38. Pichon, C.; Suaud, N.; Duhayon, C.; Guihéry, N.; Sutter, J.-P. Cyano-Bridged Fe(II)–Cr(III) Single-Chain Magnet Based on Pentagonal Bipyramid Units: On the Added Value of Aligned Axial Anisotropy. *J. Am. Chem. Soc.* **2018**, *140*, 7698–7704. [[CrossRef](#)]
39. Sommerer, S.O.; Westcott, B.L.; Cundari, T.R.; Krause, J.A. A structural and computational study of tetraaqua[2,6-diacetylpyridinebis(semicarbazone)]-gadolinium(III) trinitrate. *Inorg. Chim. Acta* **1993**, *209*, 101–104. [[CrossRef](#)]
40. Gioia, M.; Crundwell, G.; Westcott, B.L. Tetraaqua[2,6-diacetylpyridine bis(semicarbazone)]samarium(III) trinitrate. *IUCrData* **2018**, *3*, x181454. [[CrossRef](#)]
41. Sasnovskaya, V.D.; Kopotkov, V.A.; Kazakova, A.V.; Talantsev, A.D.; Morgunov, R.B.; Simonov, S.V.; Zorina, L.V.; Mironov, V.S.; Yagubskii, E.B. Slow magnetic relaxation in mononuclear complexes of Tb, Dy, Ho and Er with the pentadentate (N3O2) Schiff-base dapsc ligand. *New J. Chem.* **2018**, *42*, 14883–14893. [[CrossRef](#)]
42. Palenik, G.J.; Wester, D.W.; Rychlewska, U.; Palenik, R.C. Pentagonal-Bipyramidal Complexes. Synthesis and Crystal Structures of Diaqua [2,6-diacetylpyridine bis(semicarbazone)]chromium(III) Hydroxide Dinitrate Hydrate and Dichloro[2,6-diacetylpyridine bis(semicarbazone)] iron(III) Chloride Dihydrate. *Inorg. Chem.* **1976**, *15*, 1814–1819. [[CrossRef](#)]
43. Pascal, P. Magnetochemical studies. *Ann. Chim. Phys.* **1910**, *19*, 5–70.
44. Kahn, O. *Molecular Magnetism*; VCH Publishers: New York, NY, USA, 1993.
45. Sheldrick, G.M. SHELXT—Integrated space-group and crystal-structure determination. *Acta Cryst.* **2015**, *A71*, 3–8. [[CrossRef](#)]
46. Sheldrick, G.M. Crystal structure refinement with SHELXL. *Acta Cryst.* **2015**, *C71*, 3–8. [[CrossRef](#)]
47. Nakamoto, K. *Infrared and Raman Spectra of Inorganic and Coordination Compounds*, 4th ed.; John Wiley & Sons: Hoboken, NJ, USA, 1986; p. 245.
48. Llunell, M.; Casanova, D.; Cirera, J.; Alemany, P.; Alvarez, S. *SHAPE, Program for the Stereochemical Analysis of Molecular Fragments by Means of Continuous Shape Measures and Associated Tools, Version 2.1*; University of Barcelona: Barcelona, Spain, 2013.
49. Benelli, C.; Gatteschi, D. Magnetism of Lanthanides in Molecular Materials with Transition-Metal Ions and Organic Radicals. *Chem. Rev.* **2002**, *102*, 2369–2388. [[CrossRef](#)]
50. Kahn, M.L.; Ballou, R.; Porcher, P.; Kahn, O.; Sutter, J.-P. Analytical Determination of the {Ln–Aminoxy Radical} Exchange Interaction Taking into Account Both the Ligand-Field Effect and the Spin–Orbit Coupling of the Lanthanide Ion (Ln = DyIII and HoIII). *Chem. A Eur. J.* **2002**, *8*, 525–531. [[CrossRef](#)]
51. Guo, Y.-N.; Xu, G.-F.; Gamez, P.; Zhao, L.; Lin, S.-Y.; Deng, R.; Tang, J.; Zhang, H.-J. Two-Step Relaxation in a Linear Tetranuclear Dysprosium(III) Aggregate Showing Single-Molecule Magnet Behavior. *J. Am. Chem. Soc.* **2010**, *132*, 8538–8539. [[CrossRef](#)]

52. Grahl, M.; Kötzler, J.; Seßler, I. Correlation between Domain-Wall Dynamics and Spin-Spin Relaxation in Uniaxial Ferromagnets. *J. Magn. Magn. Mater.* **1990**, *90–91*, 187–188. [[CrossRef](#)]
53. Dolai, M.; Ali, M.; Titiš, J.; Boča, R. Cu(II)–Dy(III) and Co(III)–Dy(III) Based Single Molecule Magnets with Multiple Slow Magnetic Relaxation Processes in the Cu(II)–Dy(III) Complex. *Dalton Trans.* **2015**, *44*, 13242–13249. [[CrossRef](#)] [[PubMed](#)]
54. Lucaccini, E.; Sorace, L.; Perfetti, M.; Costes, J.-P.; Sessoli, R. Beyond the Anisotropy Barrier: Slow Relaxation of the Magnetization in Both Easy-Axis and Easy-Plane Ln(Trensal) Complexes. *Chem. Commun.* **2014**, *50*, 1648–1651. [[CrossRef](#)] [[PubMed](#)]
55. Zadrozny, J.M.; Atanasov, M.; Bryan, A.M.; Lin, C.Y.; Rekker, B.D.; Power, P.P.; Neese, F.; Long, J.R. Slow Magnetization Dynamics in a Series of Two-Coordinate Iron(II) Complexes. *Chem. Sci.* **2013**, *4*, 125–138. [[CrossRef](#)]
56. Feng, X.; Liu, J.L.; Pedersen, K.S.; Nehrkorn, J.; Schnegg, A.; Holldack, K.; Bendix, J.; Sigrist, M.; Mutka, H.; Samohvalov, D.; et al. Multifaceted Magnetization Dynamics in the Mononuclear Complex [ReIVCl<sub>4</sub>(CN)<sub>2</sub>]<sup>2-</sup>. *Chem. Commun.* **2016**, *52*, 12905–12908. [[CrossRef](#)] [[PubMed](#)]
57. Ding, Y.S.; Yu, K.X.; Reta, D.; Ortu, F.; Winpenny, R.E.P.; Zheng, Y.Z.; Chilton, N.F. Field- and Temperature-Dependent Quantum Tunnelling of the Magnetisation in a Large Barrier Single-Molecule Magnet. *Nat. Commun.* **2018**, *9*, 1–10. [[CrossRef](#)] [[PubMed](#)]
58. Liu, X.; Feng, X.; Meihaus, K.R.; Meng, X.; Zhang, Y.; Li, L.; Liu, J.; Pedersen, K.S.; Keller, L.; Shi, W.; et al. Coercive Fields Above 6 T in Two Cobalt(II)–Radical Chain Compounds. *Angew. Chem. Int.* **2020**, *59*, 10610–10618. [[CrossRef](#)] [[PubMed](#)]
59. Reta, D.; Chilton, N.F. Uncertainty estimates for magnetic relaxation times and magnetic relaxation parameters. *Phys. Chem. Chem. Phys.* **2019**, *21*, 23567–23575. [[CrossRef](#)]
60. Wang, R.; Wang, H.; Wang, J.; Bai, F.; Ma, Y.; Li, L.; Wang, Q.; Zhao, B.; Cheng, P. The different magnetic relaxation behaviors in [Fe(CN)<sub>6</sub>]<sup>3-</sup> or [Co(CN)<sub>6</sub>]<sup>3-</sup> bridged 3d–4f heterometallic compounds. *CrystEngComm* **2020**, *22*, 2998–3004. [[CrossRef](#)]